Available online at www.sciencedirect.com
ScienceDirect
Trans. Nonferrous Met. Soc. China 25(2015) 1794−1803
Transactions of Nonferrous Metals Society of China
www.tnmsc.cn

Fracture behavior of double-pass TIG welded 2219-T8 aluminum alloy joints under transverse tensile test

Quan LI[1,2], Ai-ping WU[1,2], Yue ZHAO[3], Guo-qing WANG[4], Dong-yang YAN[4], Hui-qiang WU[4]

1. Department of Mechanical Engineering, Tsinghua University, Beijing 100084, China;
2. Key Laboratory for Advanced Materials Processing Technology, Ministry of Education, Tsinghua University, Beijing 100084, China;
3. School of Aerospace, Tsinghua University, Beijing 100084, China;
4. Beijing Institute of Astronautics Systems Engineering, Beijing 100076, China

Received 25 June 2014; accepted 2 September 2014

Abstract: 2219-T8 aluminum alloys were butt welded by the double-pass tungsten inert gas (TIG) arc welding process. The transverse tensile test of the joint showed that the fracture mainly occurred in the partially melted zone (PMZ). Effects of the PMZ on the fracture behavior were systematically studied. Continuous intergranular eutectics were observed in the PMZ close to the fusion line. Away from the fusion line, the intergranular eutectics in the PMZ became discontinuous. The fracture morphology and the microhardness distribution of the joint showed that the PMZ was gradient material with different mechanical properties, which strongly affected the fracture process. It was observed that the crack initiated in the PMZ near the front weld toe, and propagated in the PMZ away from the fusion line. Then, the crack tip was blunt when it propagated into the PMZ with higher plasticity. Finally, the rest part of the joint was shear fractured.

Key words: 2219 aluminum alloy; tungsten inert gas arc welding; partially melted zone; fracture behavior

1 Introduction

Precipitation hardening 2219 aluminum alloy has been widely used in welded cryogenic fuel tanks due to its outstanding mechanical properties over a wide temperature range from −250 °C to 250 °C [1]. Friction stir welding (FSW) of 2219 aluminum alloy is a pioneer method. The joints of FSW have superior mechanical properties compared with the fusion welded joints [2,3]. However, there are still many challenge problems that need to be overcome for its fully industrial application. Fusion welding methods like variable polarity plasma arc (VPPA) [4] welding and variable polarity tungsten inert gas (VPTIG) [5] arc welding are widely used in production line due to their good flexibility and low cost. For example, double-pass welding method with tungsten inert gas (TIG) helium-arc welding as the first pass and VPTIG argon-arc welding as the second pass is one of the present welding processes in production.

The fracture of the welded joints of aluminum alloys induced by transverse load can often occur in the real structures. Therefore, transverse tensile test is one of the widely used methods to evaluate the mechanical performance of the welded joints. HUANG and KOU [6] studied the mechanical behavior of gas metal arc welded joints of 2219-T851 aluminum alloy by transverse tensile test. The results showed that the crack initiated in the partially melted zone (PMZ) and propagated along the PMZ. The weakening of the PMZ was caused by the Cu segregation. Intensive studies were conducted on the liquation and solidification mechanism of the PMZ [7,8]. SRINIVASA-RAO et al [9] studied the effects of welding technique and prior thermal temper on the liquation susceptibility of 2219 aluminum alloy. The results demonstrated that liquation susceptibility was higher in T6 temper than in T87, and pulse current technique can improve the resistance of susceptibility to liquation in PMZ. However, they are not concerned with the relationship between the microstructures of the PMZ and its fracture behavior under transverse tensile test.

The PMZ of the fusion welded 2219 aluminum alloy joint is a gradient material since its temperature field during welding is not uniform. Its fracture behavior

Corresponding author: Quan LI; Tel: +86-10-62773859-5; Fax: +86-10-62773859-5; Email: liquan10@mails.tsinghua.edu.cn
DOI: 10.1016/S1003-6326(15)63785-2

is different with homogeneous materials. In this work, 2219-T8 aluminum alloys were butt welded by the double-pass TIG welding process. The fracture of the joints under transverse tensile test mainly occurred in the PMZ. The effects of the PMZ microstructures on the fracture behavior of the joints were systematically investigated.

2 Experimental

2219-T8 aluminum alloys were used as base materials in the present work. T8 stands for solution heat treating, cold working followed by artificial aging. The dimensions of the workpieces were 300 mm × 150 mm × 6 mm. The workpieces were butt welded along the longwise (rolling) direction with 2325 (Al−Cu−Mn) filler metal, which is developed by Aerospace Research Institute of Materials & Processing Technology, China. The chemical compositions of the base material and filler metal are given in Table 1 [10].

Prior to welding, the oxide film on the base material was scraped out. Double-pass welds, with TIG helium-arc weld as the first pass and VPTIG argon-arc weld as the second pass, were made parallel to the rolling direction of the workpieces. Weld groove was not needed for this welding process. The welding parameters are given in Table 2.

After welding, the tensile samples were cut perpendicular to the weld seam according to standard ISO 6892-1:2009. The dimensions are shown in Fig. 1. A WDW-100 electronic universal testing machine was used for the tensile test. The crosshead speed was 2 mm/min. Before the tensile test, speckles were sprayed on the side face of the specimens to measure the strain field on the transverse section of the joints during the tensile test using digital image correlation (DIC) technique. The DIC device was Aramis 4M optical measuring system developed by GOM. High speed video (MEMRECAM HX-3, developed by NAC) technique was used for capturing the fracture process of the tensile specimen.

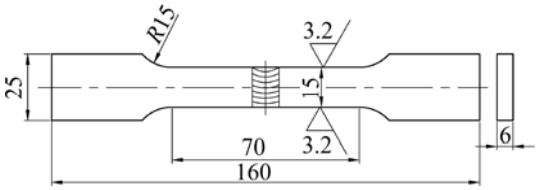

Fig. 1 Dimensions of tensile specimen (unit: mm)

The photographing speed was 5000 frame/s.

Microhardness test was conducted on MH-3 Vickers hardness tester with a 100 g load and a holding time of 10 s. Microstructure examination was carried out by optical microscopy and scanning electronic microscopy (SEM). Fracture morphology was examined with SEM. The secondary phase on the surface was analyzed by energy dispersive spectrometry (EDS).

3 Results

3.1 Fracture process of joint

During the tensile test, the welded joints always fractured suddenly while the stress−strain curves were still rising (Fig. 2). By high speed video, the joint fracture process under transverse tensile load was captured (Fig. 3). Figure 3(a) shows the photo of the joint just before the initiation of the crack. The corresponding time was set as t=0 s. At t=0.2 ms, the crack initiated in the region near the front toe, which is marked by a red rectangle in Fig. 3(b). At t=0.4 ms, the crack propagated forward along the thickness direction of the tensile sample (Fig. 3(c)). At t=0.6 ms, it is found that the crack open degree was larger and the crack stopped propagating along the primary direction. It indicates that the crack was blunt (Fig. 3(d)). Figure 3(d) also shows that the rest part of the joint was rupturing in the direction away from the primary propagation direction of the crack. The rupture speed was so high that the captured photo was out of focus. At t=0.8 ms, the ruptured joint was finally separated into two parts (Fig. 3(e)).

Table 1 Chemical compositions of base material and filler metal (mass fraction, %) [10]

Material	Si	Fe	Cu	Mn	Mg	Zn	Ti	Zr	V	Al
2219	0.2	0.3	5.8−6.8	0.2−0.4	0.02	0.1	0.02−0.1	0.10−0.25	0.05−0.15	Bal.
2325	−	−	6.0−6.8	0.2−0.4	−	−	0.1−0.2	−	−	Bal.

Table 2 Welding parameters for double-pass TIG welding of 2219-T8 aluminum alloy

Procedure	Current/A	Voltage/V	Speed/ ($mm·s^{-1}$)	Shielding gas	Flow rate/ ($L·min^{-1}$)	Filler wire	Pulse frequency/Hz
First pass	185	19	4.3	He	10	−	−
Second pass	Peak: 305−315 Base: 160	Peak: 22−23 Base:17	2.3	Ar	11−12	2325	0.8

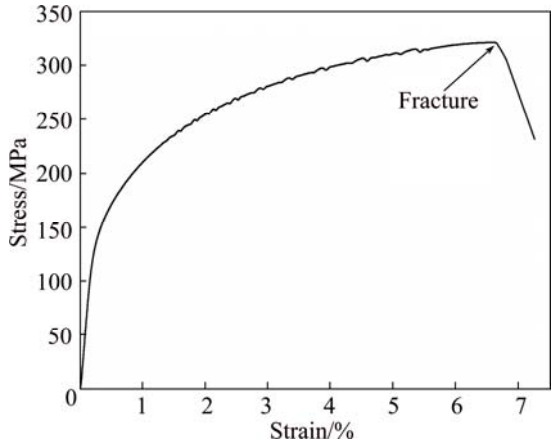

Fig. 2 Stress−strain curve of double-pass TIG welded joints under transverse tensile test

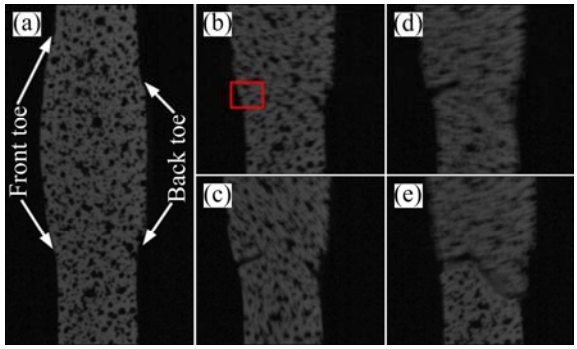

Fig. 3 High speed video photos of tensile specimen: (a) Before crack initiation, t=0 s; (b) Crack initiation, t=0.2 ms; (c) Crack propagation, t=0.4 ms; (d) Fast rupturing, t=0.6 ms; (e) Separating, t=0.8 ms

3.2 Strain field of joint before fracture

The typical cross section of the joint after tensile test is shown as Fig. 4(a). The boundaries of different regions are indicated by red curves. The strain distribution on the side face of the joint just before the occurrence of fracture is shown in Fig. 4(b). Combining Fig. 4(b) with Fig. 4(a), it is found that the strain concentrated in the region near the fusion line and the over aged zone (OAZ). According to the microhardness distribution of the joint (shown in Fig. 5), the hardness of the fusion zone was the lowest and that of the OAZ was a little higher. For compensating the strength loss of the weld, the weld reinforcement remained. Due to the effect of the reinforcement, the deformation near the fusion line was larger than that of the fusion zone center. Comparing the fracture position with the strain field, it is found that the crack initiated in the region near the front toe, where an obvious deformation concentration existed. After the crack was initiated, it propagated away from the deformation concentrated region or the fusion line. At the front toe, the distance from the crack to the fusion line was 373 μm (Fig. 6). When the distance came to

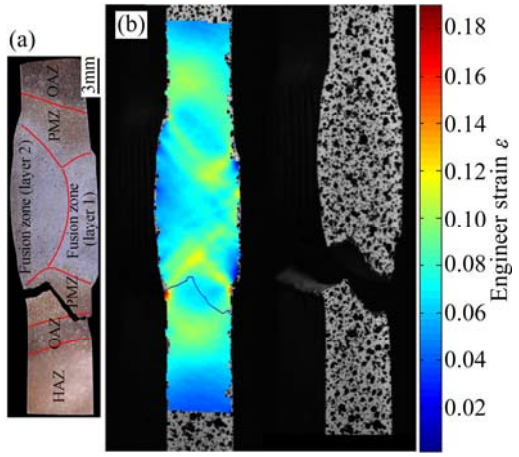

Fig. 4 Metallurgical graph of joint after rupture (a) and strain field of joint's side face before fracture (b)

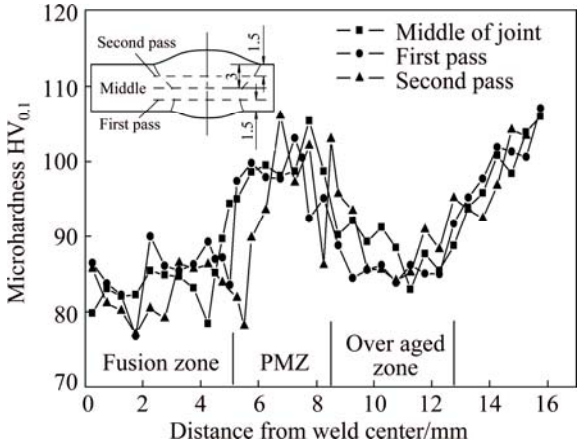

Fig. 5 Microhardness distribution of transverse section of joint

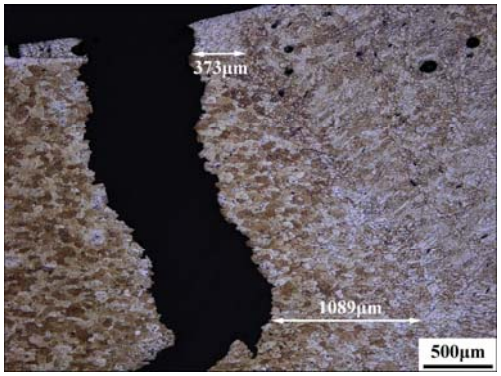

Fig. 6 Optical graph of upper fracture section of joint

1089 μm, the crack was blunt. According to the microhardness distribution shown in Fig. 5, the crack propagated in the PMZ and the strength of the material around the crack tip increased with the distance from it to the fusion line. It demonstrated that the crack propagated in a gradient material before it was blunt. The rest fracture path was also mainly located in the PMZ which presented a high strength according to the microhardness distribution. The strain distribution

indicates that the deformation in this region before fracture was small as shown in Fig. 4(b). It is interesting that the joint mainly fractured in the PMZ with low deformation, and there was an obvious crack blunt point on the fracture path.

3.3 Microstructure of fracture section of joint

As mentioned above, the fracture path was mainly in the PMZ of the joint. Figure 7 shows the low magnification microstructure of the PMZ near the fusion line. There were thin secondary phases at the grain boundaries forming like networks. More continuous and thicker secondary phases were observed close to the fusion line.

The high magnification photos of the PMZ microstructure are shown in Fig. 8. The EDS analysis results of the PMZ are shown in Table 3. In the region near the fusion line (Figs. 8(a) and (b)), coupled eutectics formed within the grains. The Cu/Al mass ratio of position M_1 in Fig. 8(b) was 26.43:72.92 (Table 3), which was close to the chemical composition of the coupled eutectic α(Al)+θ(Al_2Cu) (m(Cu)/m(Al)=33:67). The coupled eutectic formed due to the liquation reaction of the residual θ(Al_2Cu) in base material with the surrounded α(Al) substrate, which is widely accepted [7,9]. The grain boundary was mainly composed of divorced eutectics (θ phase) and some coupled eutectic particles, which were the consequence of grain boundary liquation. Position M_2 in Fig. 8(b) at the grain boundary was an intergranular coupled eutectic particle with a very close Cu/Al mass ratio (Table 3) to 33:67. Since the divorced eutectics were very thin, their accurate compositions were hard to be detected by EDS. To date, the grain boundary liquation mechanism is still a controversial issue [7,11−13].

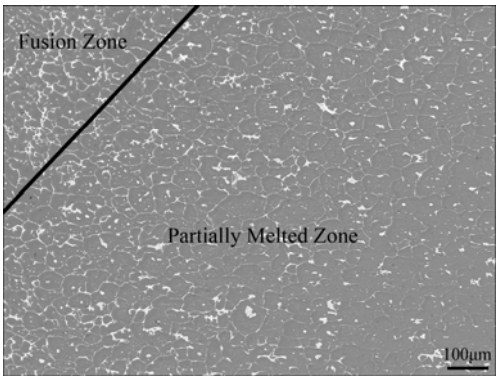

Fig. 7 Low magnification back scatter electronic image of PMZ microstructure

In the PMZ boundary region about 3 mm away from the fusion line, there were two kinds of secondary phases: θ phase (m(Cu)/m(Al)=53:47) and coupled eutectic particle (Figs. 8(c) and (d)), which were confirmed by the EDS results (positions M_5 and M_6 in Fig. 8 (d)). It indicates that the peak temperature during welding in this region was close to the eutectic reaction temperature. In addition, Cu concentration of the α(Al) substrate in the PMZ boundary (position M_7) is higher than that of the PMZ near the fusion line (positions M_3 and M_4).

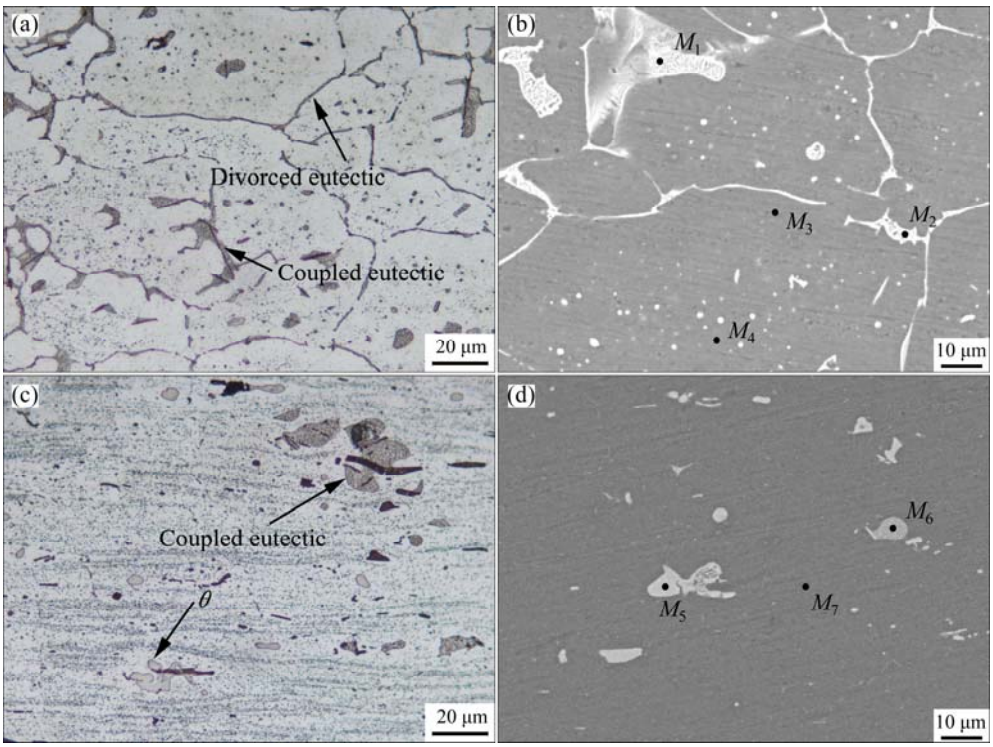

Fig. 8 Microstructures of PMZ near fusion line: (a) Optical image; (b) BSE image showing microstructure of PMZ boundary: (c) Optical image; (d) BSE image

Table 3 EDS analysis results of different positions in PMZ of Fig. 8 (mass fraction, %)

Element	M_1	M_2	M_3	M_4	M_5	M_6	M_7
Cu	26.43	31.44	3.43	4.14	47.22	35.95	5.98
Al	72.92	68.56	96.57	95.86	52.78	64.05	94.02
Fe	0.65						

With the peak temperature decreasing from the region near the fusion line (about 643 °C) to the PMZ boundary (about 543 °C) [10], the amount of divorced eutectics in the grain boundary decreased gradually, and finally only the coupled eutectic particles were found in the PMZ far away from the fusion line.

The optical microstructures of the joint fracture section are shown in Fig. 9. In the crack initiation region in Figs. 9(a) and 9(b), eutectics distributed continuously along the grain boundaries and formed like networks. Intergranular fracture was visible, and some fragmentized eutectic particles still remained on the fracture boundary (Fig. 9(b)). During the tensile load, a lot of microcracks were produced since the intergranular

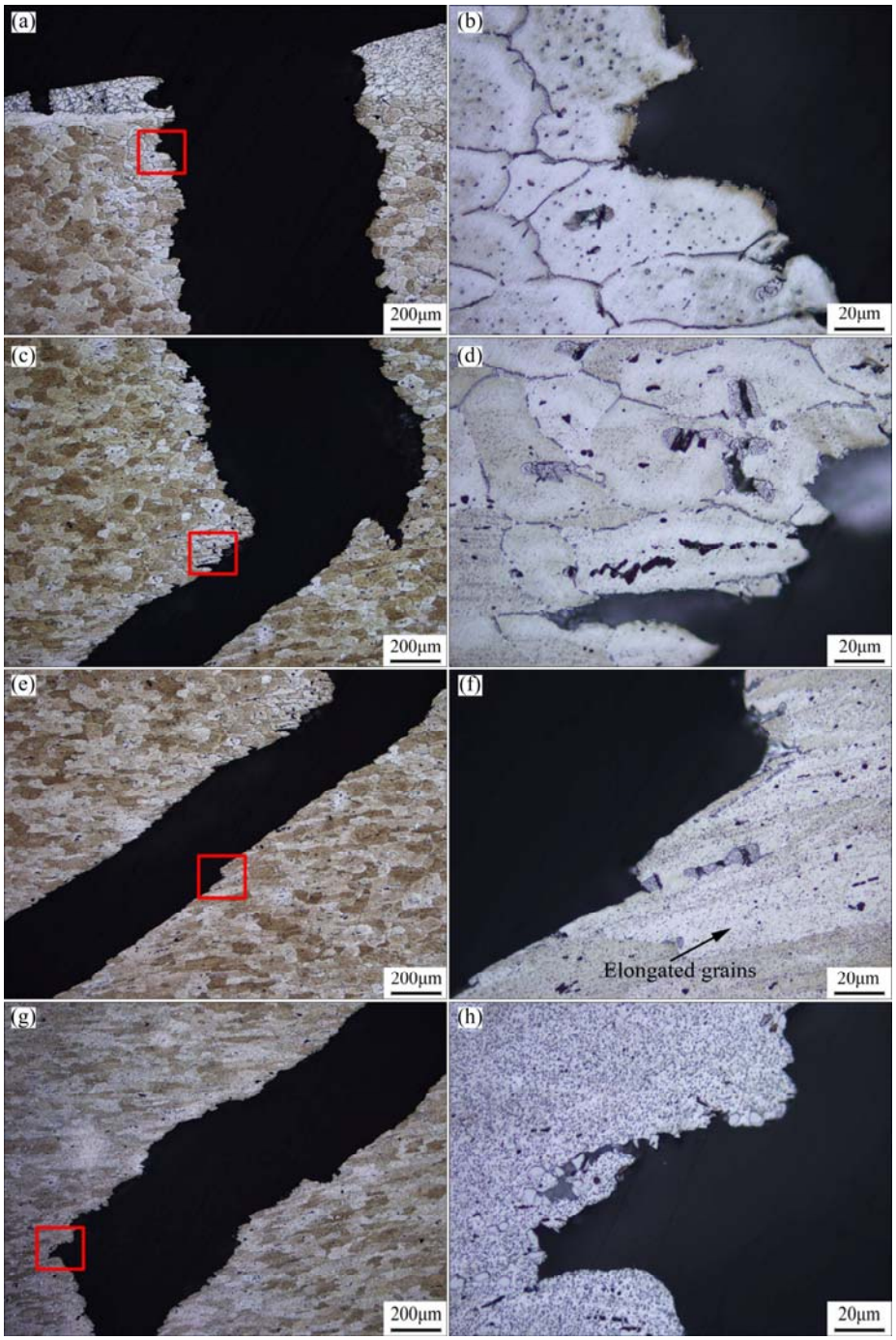

Fig. 9 Microstructures of fracture section in crack initiation region (a, b), crack blunt region (c, d), shear fracture region of PMZ (e, f) and shear fracture region of over aged zone (g, h)

brittle eutectics deformed inconsistent with the α(Al) matrix. These microcracks may coalescence as macro cracks with the tensile load carrying on. Therefore, the intergranular eutectics deteriorated the plasticity of the PMZ materials. In the crack blunt region (Fig. 9(c)), the distance of the crack to fusion line was longer than that of the crack initiation region. The intergranular eutectics became discontinuous and their thickness was thinner than those in the crack initiation region (Fig. 9(d)). The plasticity of this region should be better than that of the crack initiation region since the amount of intergranular eutectic decreased. So, the brittle fracture mode stopped when the crack propagated into this region. Because of the large plasticity deformation around the crack tip in this region during the fracture, the grain interior coupled eutectic particles were fractured (Fig. 9(d)). Below the crack blunt region, it is observed that the grains were elongated toward the fracture direction (Figs. 9(e) and (f)), which demonstrated that the grains experienced a large deformation before the fracture. The elongation of the grains indicated that the rest part of the joint fractured in the shear mode. The fracture sheared across the PMZ (Figs. 9(e) and (f)) and the OAZ (Figs. 9(g) and (h)). In the PMZ side, the fracture of coupled eutectic particles during plastic deformation formed the microvoids (Fig. 9(f)), while they were formed by the fracture of θ phase or the decohesion of θ phase with α(Al) matrix in the OAZ (Fig. 9(h)). The growth and coalescence of these microvoids contributed to the macro shear fracture.

3.4 Fracture morphology of joint

The different fracture characteristics on the microstructure of the fracture section of the joint are also reflected on the fracture morphology of the joint. In the crack initiation region (Fig. 10(a)), the proportion of tear ridges and dimples on the fracture surface was small. Some brittle fractured particles on the bottom of the shallow tear ridges were visible (Fig. 10(b)). The EDS analysis results (Table 4) indicate that these particles (positions F_1 and F_2 in Fig. 10(b)) were coupled eutectics α(Al)+θ(Al_2Cu). The lamellar eutectic morphology can be clearly observed at position F_1 in Fig. 10(b). The fracture morphology of the crack initiation region indicates that the material in this region was brittle. In the crack blunt region (Fig. 10(c)), the proportions of tear ridges and dimples on the fracture surface were higher than those in the crack initiation region, which demonstrates that this region had a better plasticity property. At the bottom of the tear ridges, eutectic particles were also visible (positions F_4 and F_5 in Fig. 10(d)). In the shear fracture region of PMZ (Figs. 10(e) and (f)), the fracture surface was full of dimples with eutectic particles at the bottom (positions F_7 and F_8 in Fig. 10(f)). In the shear fracture region of OAZ (Figs. 10(g) and (h)), the fracture was composed of many small and large dimples. At the bottom of large dimples, the residual θ phases were found (positions F_{10} and F_{11} in Fig. 10(h)). The fracture morphologies of the shear fracture region of PMZ and OAZ reveal that the plasticity property of these regions was greater than that of the crack initiation region and the crack blunt region. As mentioned above, the eutectics or θ particles in this region were the source to form microvoids for shear fracture.

Table 4 EDS analysis results of different positions on fracture of joint in Fig. 10 (mass fraction, %)

Position	Cu	Al	Fe
F_1	30.35	66.92	2.73
F_2	34.07	65.93	−
F_3	4.52	95.48	−
F_4	19.23	80.77	−
F_5	46.37	53.63	−
F_6	8.48	91.52	−
F_7	38.12	61.88	−
F_8	28.52	71.48	−
F_9	7.96	92.04	−
F_{10}	51.67	48.33	−
F_{11}	26.18	68.51	5.31
F_{12}	7.68	92.32	−

4 Discussion

4.1 Crack initiation

The ultimate tensile strength of the weld joints depends on the crack initiation resistance of the joint since the joints fail before necking. Crack initiation is influenced by the stress state and microstructure in the crack initiation region. Since the crack initiation region was near the weld toe for the free flaw weld, the stress state was affected by the transition angle and radius of the weld toe. Moreover, the fusion line angle near this region can also influence the crack initiation. Due to the overflow of weld metal during welding, the weld toe is always located on the PMZ near the fusion line. The width of PMZ is about 3 mm and the microstructures in the PMZ are different due to the different thermal histories. The microstructures near the weld toe are composed of intergranular network eutectics and some intragranular coupled eutectic particles because of the liquation of grain boundary and θ particles.

The thickness and continuous degree of the intergranular eutectics may largely affect the crack initiation resistance of the PMZ. During the tensile test, microcracks form in the eutectics due to their low resistance to deformation compared with α(Al) matrix as

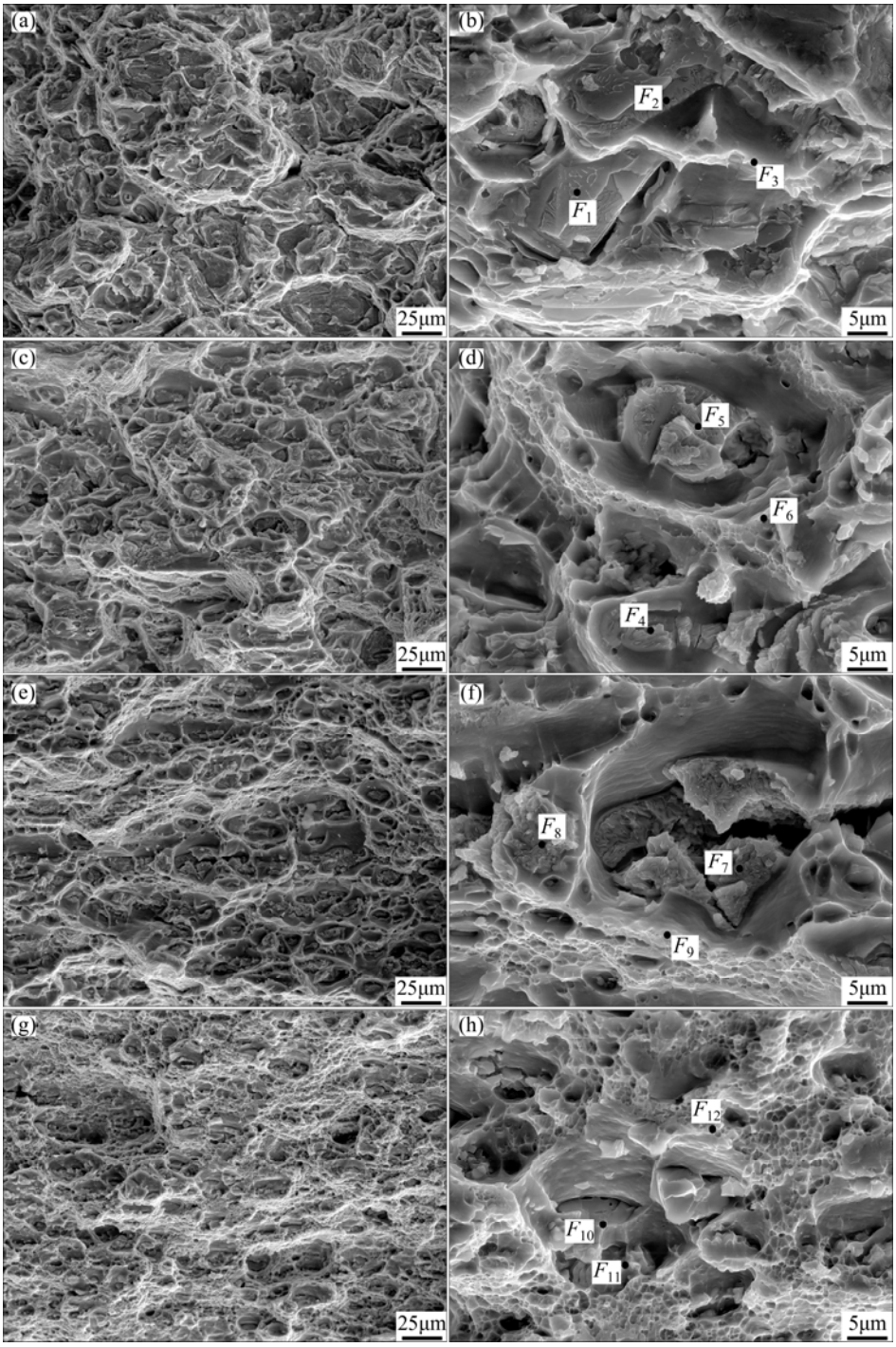

Fig. 10 Secondary electronic images of fracture morphology in crack initiation region (a, b), crack blunt region (c, d), shear fracture region of PMZ (e, f) and shear fracture region of over aged zone (g, h)

illustrated in Fig. 11. Particle *A* (Fig. 11) was an isolate intragranular eutectic particle, which fractured perpendicular to the tensile direction. However, the propagation of the microcrack in particle *A* was prohibited by the surrounded α(Al) matrix because of their good plasticity. Larger crack or cavity under the tensile load can easily form in the thick and continuous intergranular eutectics as indicated by arrows *B* and *C* in Fig. 11. The coalescence of these intergranular microcracks may evolve into a macrocrack. Thus, some fragmentized eutectics remained on the fracture boundary in the crack initiation region as shown in Fig. 9(b). The PMZ microstructures near the front toe and the back toe are shown in Fig. 12. The intergranular eutectics of the PMZ near the front toe were larger and more continuous than those of the PMZ near the back toe. This is because the heat input of the second pass was larger than that of the first pass. Thus, the crack initiation

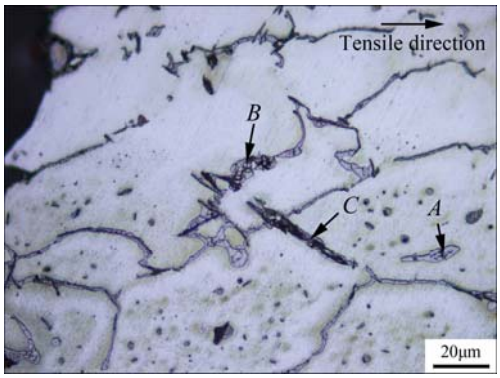

Fig. 11 Microstructure near fracture in crack initiation region

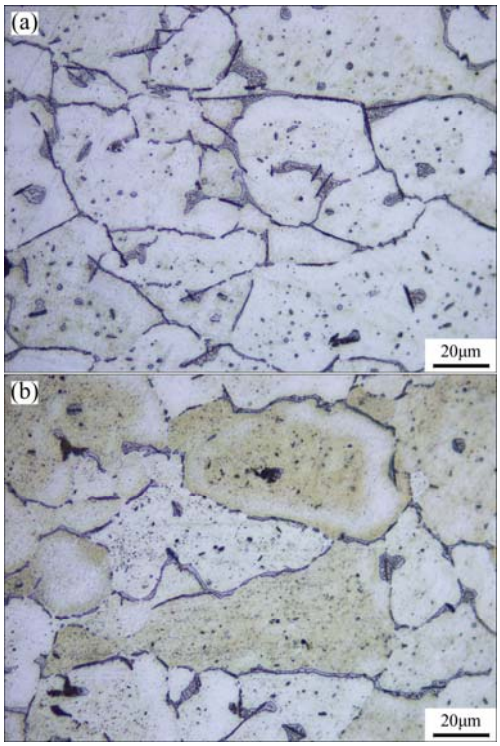

Fig. 12 Optical microstructures of PMZ near front toe (a) and back toe (b)

resistance of the PMZ microstructure near the front toe was smaller. The weak region of the joint was the PMZ near the front toe and crack initiated in this region.

4.2 Crack propagation

According to the microhardness distribution shown in Fig. 5, the PMZ can be divided into two regions, i.e., PMZ I and PMZ II as shown in Fig. 13. In PMZ I, the microhardness increased from about HV 85 at the fusion line to HV 100 at the location of 1 mm away from the fusion line. Due to the effect of intergranular eutectics, PMZ I can be termed as quasi-brittle materials. The rest part of PMZ is regarded as PMZ II with better strength and plasticity. Supposing there is a crack initiated in PMZ I near the front toe as shown in Fig. 13. The tangential stress around the crack tip (point G) at point *P* in PMZ I can be calculated as the following equation [14,15]

$$\sigma_\theta=\frac{\cos(\theta/2)}{2\sqrt{2\pi r}}\left[K_{\mathrm{I}}\left(1+\cos\theta\right)-3K_{\mathrm{II}}\sin\theta\right] \quad (1)$$

where r and θ are the polar coordinates of point P shown in Fig. 13, K_{I} and K_{II} are the stress intensity factors of mode I and mode II cracks, respectively, defined as

$$K_{\mathrm{I}}=\sigma^2\sin^2\beta\sqrt{\pi a}F \quad (2)$$

$$K_{\mathrm{II}}=\sigma^2\sin\beta\cos\beta\sqrt{\pi a}F \quad (3)$$

where σ is the tensile stress far away from the crack, β is the crack angle (Fig. 13), a is the crack length and F is a configuration factor which accounts for the proximity effects of boundary surfaces [16].

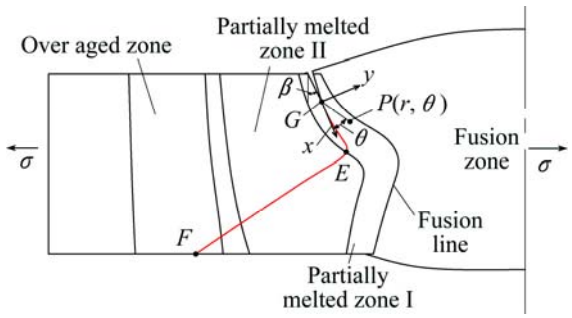

Fig. 13 Schematic crack propagation of joint under transverse tensile load

For homogeneous materials, the crack will propagate in the direction when the tangential stress is the maximum value [15]. In order to meet this requirement, θ should be a negative value θ_{n} according to Eq. (1). For imhomogeneous materials like the gradient PMZ I, θ is not equal to θ_{n} under the effect of varied strength in different directions around the crack tip. With the decreasing of θ from $\pi/2$ to θ_{n}, the tangential stress σ_θ increases as well as the strength of the materials at point P (r, θ). If θ is close to $\pi/2$, σ_θ may be too small, and the crack cannot propagate in this direction. If θ is close to θ_{n}, the strength of the material may be too large, and the crack also cannot propagate in this direction. So, for the welded joints in this work, the crack will propagate in a certain direction between $\pi/2$ and θ_{n}, in which direction σ_θ is large enough and the strength of the material is not too large. Over all, the strength gradient plays a key role in the propagation of the crack in PMZ I.

4.3 Rupture

Once the crack propagates into PMZ II (point *E* in Fig. 13), which is about 1 mm away from the fusion line and has good plasticity and strength, Eq. (1) is no longer suitable to control the crack propagation. Due to the plasticity deformation around the crack tip, the crack tip

is blunt at point *E* as shown in Fig. 13. As the microstructure of the fracture section shown in Fig. 9 and the fracture morphology shown in Fig. 10, the microstructure along line *EF* will experience a large deformation and fracture in the shear mode instantly.

4.4 Suggestion for improving mechanical properties of joints

According to the above analysis, the tensile property of the welded joint is determined by the crack initiation resistance of the PMZ region near the front toe. The microstructure of this region is one of the key factors that affect the tensile strength of the joint. The crack initiation resistance of the PMZ decreases with the increase of the thickness and continuous degree of the intergranular eutectics. The intergranular eutectics morphology is determined by the peak temperature, heating rate and cooling rate of the thermal cycle in the PMZ. In order to decrease the heat effect on the microstructure of the PMZ, the heat input of the second pass should be decreased while the energy density should be increased.

5 Conclusions

1) The fracture of the double-pass TIG welded 6 mm 2219-T8 aluminum alloy joint under transverse tensile test occurred in the PMZ. The PMZ was a gradient material. Continuous intergranular eutectic phases were observed in the PMZ close to the fusion line. Away from the fusion line, the intergranular eutectic phases became discontinuous.

2) The fracture behavior was strongly affected by the mechanical properties of different PMZ regions. The crack initiated in the PMZ near the front toe of the joint, where the plasticity property of the PMZ is low. Then, the crack propagated in the PMZ away from the fusion line. When the crack propagated into the PMZ 1 mm away from the fusion line, the crack tip was blunt since the materials around the crack tip had a good plasticity property. Finally, the rest part of the joint was shear fractured. The fracture morphology of the shear fracture region revealed that the plasticity property of these regions was greater than that of the crack initiation region and the crack blunt region.

3) The weak region of the welded joint was the PMZ near the front toe. Intergranular eutectics in PMZ had an important effect on the resistance ability to crack initiation. The crack initiation resistance of the PMZ decreased with the increase of the thickness and continuous degree of the intergranular eutectics.

4) The crack propagation direction was affected by the strength gradient of the PMZ near the fusion line before the crack was blunt.

References

[1] VENKATA-NARAYANA G, SHARMA V M J, DIWAKAR V, SREE-KUNA K R, PRASAD R C. Fracture behaviour of aluminium alloy 2219−T87 welded plates [J]. Science and Technology of Welding and Joining, 2004, 9(2): 121−130.

[2] XU Wei-feng, LIU Jin-he, LUAN Guo-hong, DONG Chun-lin. Microstructure and mechanical properties of friction stir welded joints in 2219-T6 aluminum alloy [J]. Materials & Design, 2009, 30(9): 3460−3467.

[3] CHEN Ying-chun, LIU Hui-jie, FENG Ji-cai. Friction stir welding characteristics of different heat-treated-state 2219 aluminum alloy plates [J]. Materials Science and Engineering A, 2006, 420(1−2): 21−25.

[4] WANG H X, WEI Y H, YANG C L. Numerical simulation of variable polarity vertical-up plasma arc welding process [J]. Computational Materials Science, 2007, 38(4): 571−587.

[5] DING Ji-kun, WANG Dong-po, WANG Ying, DU Hui. Effect of post weld heat treatment on properties of variable polarity TIG welded AA2219 aluminium alloy joints [J]. Transactions of Nonferrous Metals Society of China, 2014, 24(5): 1307−1316.

[6] HUANG C, KOU S. Partially melted zone in aluminium welds: Solute segregation and mechanical behaviour [J]. Welding Journal, 2001, 80(9): 9−17.

[7] HUANG C, KOU S. Partially melted zone in aluminum welds—Liquation mechanism and directional solidification [J]. Welding Journal, 2000, 79(5): 113−120.

[8] HUANG C, KOU S. Partially melted zone in aluminum welds—Planar and cellular solidification [J]. Welding Journal, 2001, 80(12): 46−50.

[9] SRINIVASA-RAO K, MADHUSUDAN-REDDY G, PRASAD-RAO K. Studies on partially melted zone in aluminium–copper alloy welds—Effect of techniques and prior thermal temper [J]. Materials Science and Engineering A, 2005, 403(1): 69−76.

[10] DAVIS J R. Aluminum and aluminum alloys [M]. Materials Park, OH: ASM International, 1993: 662−663.

[11] KUO M, FOURNELLE R A. Diffusion induced grain boundary migration (DIGM) and liquid film migration (LFM) in an Al−2.07wt% Cu alloy [J]. Acta Metallurgica et Materialia, 1991, 39(11): 2835−2845.

[12] MEYER B C, TEMPUS G, DOYEN H, EMANOWSKI D, HIRSCH T, MAYR P. Dispersoid-free zones in the heat-affected zone of aluminum alloy welds [J]. Metallurgical and Materials Transactions A, 2000, 31(5): 1453−1459.

[13] TIAN Zhi-ling, XU Liang-hong, PENG Yun, ZHANG Xiao-mu, LI Ran. Formation mechanics of the precipitate-free zone in high strength aluminum alloy welds [J]. Acta Metallurgica Sinica, 2008, 44(1): 91−97. (in Chinese)

[14] GU P, ASARO R J. Cracks in functionally graded materials [J]. International Journal of Solids and Structures, 1997, 34(1): 1−17.

[15] KHAN S M A, KHRAISHEH M K. Analysis of mixed mode crack initiation angles under various loading conditions [J]. Engineering Fracture Mechanics, 2000, 67(5): 397−419.

[16] MEGUID S A. Engineering fracture mechanics [M]. London: Elsevier Applied Science, 1989: 135.

2219-T8 铝合金单面两层焊接头横向拉伸断裂行为

李 权[1,2]，吴爱萍[1,2]，赵 玥[3]，王国庆[4]，鄢东洋[4]，吴会强[4]

1. 清华大学 机械工程系，北京 100084；
2. 清华大学 先进成形制造教育部重点实验室，北京 100084；
3. 清华大学 航空航天学院，北京 100084；
4. 北京宇航系统工程研究所，北京 100076

摘 要：采用单面两层钨极氩弧焊工艺焊接 2219-T8 铝合金。接头横向拉伸时断裂发生在部分熔化区(PMZ)。针对 PMZ 组织对接头拉伸断裂行为的影响进行系统研究。PMZ 中靠近熔合线的位置晶界共晶较连续，随着距离熔合线距离的增加，晶界共晶的连续程度逐渐降低。断口形貌和接头显微硬度分布表明 PMZ 是一种梯度材料。其梯度变化的力学性能对接头的断裂行为有重要影响。研究发现，裂纹在靠近正面焊趾的 PMZ 启裂，启裂后沿远离熔合线的方向扩展，当裂纹尖端扩展到塑性较好的 PMZ 时，裂纹尖端钝化，随后接头余下部分以剪切形式发生断裂。

关键词：2219 铝合金；钨极氩弧焊；部分熔化区；断裂行为

(Edited by Yun-bin HE)